A technique for the ultrasonic dispersion of larger quantities of cellulose nanocrystals with in-line validation

Mélanie Girard[a,b], François Bertrand[b], Jason R. Tavares[a], Marie-Claude Heuzey[a]

[a] *Research Center for High Performance Polymer and Composite Systems (CREPEC), Department of Chemical Engineering, Polytechnique Montreal, Montreal, Quebec, H3C 3A7, Canada*

[b] *Research Center for Industrial Flow Processes (URPEI), Polytechnique Montreal, Montreal, Quebec H3C 3A7, Canada*

Abstract: Cellulose nanocrystals (CNCs) can be used in a wide range of applications due to their unique properties. However, the dispersion required to achieve these properties in various media may be quite challenging, especially at larger scales. Starting from an optimized protocol to prepare small volumes (60 mL) of aqueous suspensions, a semi-continuous setup is developed in this work to disperse larger quantities (200 mL). Using this technique, a higher efficiency is achieved, consuming only 35 % of the energy needed with a comparable batch method. To follow the dispersion state, an in-line process rheometry technique is adapted and validated through finite element simulation. While this allows for fast and easy validation, a deeper analysis may also be carried out to extract additional information such as the process viscosity. This setup is further exploited for the CNC surface modification using polyethylenimine. Although it has been designed for CNCs, it may be adapted for other nanoparticle dispersion.

Keywords: Ultrasonication, cellulose nanocrystals, suspension, dispersion, in-line measurement, semi-continuous setup

1. Introduction

Cellulose nanocrystals (CNCs) are bio-based material displaying several valuable properties attributed to their surface chemistry and their nano-rod morphology. They find applications in mechanical reinforcement, optical films, 3D printing and Pickering emulsions, to name only a few [1-4].

CNCs are obtained from acid hydrolysis of cellulose fibers, removing the amorphous portion of the fibers. This may be carried out using hydrochloric or sulfuric acid (HCl or H_2SO_4). The choice of the acid will impact on the particle size [5-7], and the surface chemistry: H_2SO_4, compared to HCl, promotes dispersion in water by generating charged sulfate half-ester groups on the CNC surface [8, 9]. After hydrolysis, the CNCs may then be neutralized to improve stability or facilitate dispersion, depending on the counterion being used [10, 11]. Neutralization is generally followed by a drying phase, with typically spray-drying or freeze-drying methods. Spray-drying requires less energy and results in a more compact powder – this leads to higher crystallinity and better thermal stability [12, 13]. However, for both drying strategies, CNCs form aggregates or flakes. The bond strength within these may reach up to 10^9 Pa for the smallest particles (0.5 μm in diameter when spherical) [14]. Thus, a powerful technique is crucial to redisperse CNCs and benefit from all their properties. By

providing an energy density up to 10^8 J/m^3 ~~(Pa)~~ [15], ultrasonication is the most commonly used method at the lab scale, for efficient dispersion in low-viscosity media. High-pressure homogenization may alternatively be employed, but it requires a less ubiquitous and more expensive infrastructure.

For CNC dispersion, ultrasonication probes are favored compared to baths, offering a greater efficiency through direct contact [16]. The probes are made of a piezoelectric material, inducing pressure waves in the liquid via mechanical vibration at high frequencies. Vacuum bubbles are formed because of the alternating positive and negative pressures. Negative pressure leads to bubble growth whereas these are compressed at positive pressure. Cavitation takes place at high intensities once the bubbles are large enough (with a diameter of 170 μm for ultrasonication at 20 kHz in water). The cavities are thus able to absorb a very high amount of energy during the growing cycle, which is violently released by implosion of the bubble - local temperatures and pressures up to 5000 K and 100 bars are possible. Implosion leads to shock waves that may erode or break the CNC agglomerates. Sometimes, a cavitation "microjet" (jet induced by a small bubble collapse) is also formed near a solid boundary but only particles smaller than 200 μm will be affected [17, 18].

Batch ultrasonication protocols have recently been optimized and better understood for CNCs dispersion in water [19, 20]. These works demonstrated that the most efficient probe position is off-centered, in the upper part of the tank. Moreover,

CNC addition must be carried out carefully to avoid gelation on the surface or on the container walls (half the desired water is added before the CNC powder, followed by the remaining water content). However, sonicating larger suspension volumes leads to increasing dead zones, this process must be thus limited to small quantities (~60 mL maximum) [19]. This dead zone problem is accentuated for more viscous media, as the size of active region below the probe is decreased. However, being able to work at a much larger scale is essential to tackle industrial applications. Increasing the probe size may not be efficient as higher power is needed to provide the same intensity in a larger probe [21]. Moreover, a higher power will lead to important mechanical, electrical and heat losses, impacting the efficiency of the process. Large probes are thus usually limited to smaller amplitudes. Industrial Sonomechanics (a firm specialized in ultrasonic technology) suggests a barbell horn to overcome this problem, able to treat volumes larger than 2 L, but remains around 5 times more expensive that the traditional probe [22, 23]. To the authors' knowledge, two other solutions are currently offered at a varying cost based on ultrasonication probe technology. In the first case, the suspension to be dispersed flows in a pipe and several sonication probes are set up in series or in parallel [22]. This process increases the residence time of the suspension in active dispersion zones without increasing the overall process time. The second case is a continuous flow ultrasonication: the fluid is recirculated using a pump between a tank and a flow cell in which ultrasonication is applied. This method has been proven to be more efficient than batch sonication, both in terms of energy and time [24, 25]. In all

cases, however, an external validation procedure is required to confirm the dispersion state.

In-line measurements could thus be relevant. A useful technique has been patented to extract the properties of a power-law fluid under laminar flow (flow and consistency index n and m, process viscosity μ_{pr}) through two static mixers [26, 27]. This method is based on the Metzner-Otto concept that will be detailed in Section 2.8 [28].

Well dispersed CNCs may then be further used to prepare Pickering emulsions, achieve surface modification or solvent exchange. For example, Khandal et al. carried out polyethyleneimine (PEI) physical adsorption surface modification by adding PEI to CNC aqueous suspensions during ultrasonication. The PEI's charged amine groups were successfully electrostatically bounded to the charged sulfate groups of CNC after adequate dispersion of the particles in aqueous media [29].

Therefore, this work proposes a method to disperse larger volumes of CNCs using in-line validation. After presenting our setup composed of a semi-continuous system allowing for recirculation between a small ultrasonication vessel and a larger tank, in-line pressure measurements are used to determine the dispersion state. External conductivity and rheology are employed afterwards to validate our conclusions. Then, process viscosity is extracted from the pressure measurements, allowing confirmation of the dispersion state without external experiments. Finally,

surface modification using PEI is performed to demonstrate the expanded potential of this work.

2. Methodology

2.1. Materials

CNCs, derived from sulfuric acid hydrolysis and neutralized by a sodium counterion, were supplied in a spray-dried form by Celluforce. Their density is around 1540 $kg.m^{-3}$ and their sulfur over carbon S/C atomic ratio is ~0.0057 [13] or 211 $mmol.kg^{-1}$.

Branched PEI was purchased from Sigma-Aldrich. It has an average molecular weight of 25,000 $g.mol^{-1}$, a polydispersity of 2.5 and a density of 1030 $kg.m^{-3}$ at 25 °C.

2.2. Semi-continuous setup

Figure 1 depicts the semi-continuous setup. A 250 mL beaker (beaker A) is plugged to a pump (Hffheer – 5 V water pump – 120L/h flow rate) and used to mix CNCs coarsely in water and help the particle wetting process. This pump recirculates a portion of the fluid back to beaker A. The other part goes to a small 100 mL beaker (beaker B) using a peristaltic pump (Cole Parmer Master Flex model no. 7520-35 with the head model no. 7016-20 and Masterflex 96400-16 tubing) to control the flow rate. The ultrasonic probe (Cole-Parmer - CP505, 20 kHz with a 12.7 mm probe) is immersed in beaker B (process details may be found in Section 2.3). The sonicated fluid is sent back to beaker A using a second identical peristaltic head (mounted on the same pump

to ensure an identical flow rate). This stream is monitored through two gauged pressure sensors (NPX - MPXV7002GP, calibrated as explained in Supplementary information 2). A static mixer is installed between the two pressure sensors to increase the pressure drop. This static mixer is a 3D-printed model equivalent to a KM-Kenics mixer with helical elements, each rotating 90° from the previous one (Figure S3). The pressure sensor data are acquired with an Arduino board and a LabView interface. The tubes (Tygon ND-100-65) present an internal diameter D of 4.8 mm (3/16'').

A cooling system (blue area in Figure 1) was added around beaker B and before the first pressure sensor with 5 °C water circulation to prevent overheating. The temperature in the system was stable at 35 °C. Moreover, an air filtration system (Dri-Eaz DefendAir HEPA) is employed during CNC addition for safety issues.

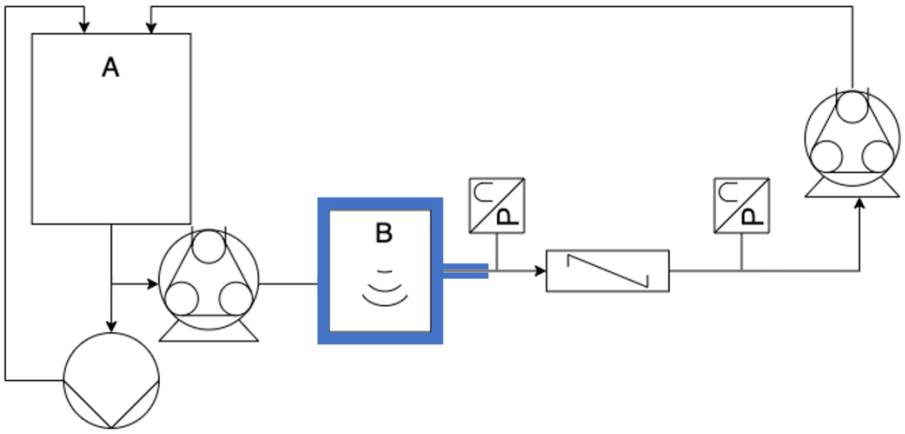

Figure 1: Semi-continuous setup schematic where A is a 250 mL beaker, B a 100 mL beaker and P the pressure sensors. Blue area corresponds to the cooling system.

2.3. CNC suspension preparation

In a previous article [19], we demonstrated that 167 $kJ.g^{-1}.L^{-1}$ (grams of CNC and liter of suspension) were necessary to achieve a well-dispersed CNC suspension in a 60 mL batch process. This required the probe to be placed at 1/3 of the total volume height and off-centered such that r/R=0.3 (where r is the probe position and R the beaker radius). Moreover, the necessary power was set to 65 W, balancing ultrasonication efficiency with the time needed to complete dispersion. These guidelines (power and probe position) have been followed in this work for a total volume of 200 mL. Three concentrations (1.6 wt%, 3.2 wt% and 4.8 wt%) have been tested. They are named respectively CNC-1.6, CNC-3.2 and CNC-4.8 (Table 1). The CNC addition rate has been set around 30 mg/10 s to ensure time for wetting and avoid exaggerate agglomeration. Accordingly, the flow rate Q controlled by the peristaltic pump has been set such that the residence time t_R in beaker B is half the one required to disperse the same amount of CNC in a batch process t_{R^*}. Indeed, if $t_R = 0.5t_{R^*}$, and $Q = 3.8*10^{-7}$ $m^3.s^{-1}$, the concentration of CNC in beaker B will reach up to 0.725 wt% if no stagnant zone is assumed during one cycle (9 minutes, corresponding to the CNC addition time for CNC-1.6), which is half of the CNC-1.6 concentration. Further addition increases proportionally the concentration. Even if the CNC concentration gets higher by homogenization after the end of CNC addition, CNCs would have already been mostly

de-agglomerated. The dispersion state is monitored with the pressure drop values – when it reaches a plateau, the suspension is considered well-dispersed.

It must be noted that ultrasonication was used in a pulse mode (8 s ON - 2 s OFF) to avoid excessive damage of the probe as the treatment is quite long.

Table 1: CNC suspension parameters.

Name	Concentration (wt%)	Addition time (min)
CNC-1.6	1.6	9
CNC-3.2	3.2	18
CNC-4.8	4.8	27

For comparison purpose, the same concentrations have been prepared using a batch process and are noted CNC-1.6*, CNC-3.2* and CNC-4.8*. All dispersion parameters were kept the same except the volume which was 60 mL in the batch process. The final dispersion state is achieved when applying 167 $kJ.g^{-1}.L^{-1}$, as per [19].

2.4. Newtonian and power-law fluids preparation

Newtonian and power-law fluids are prepared to validate the experimental setup's parameters as they have predictable behaviors. Thus, three glycerol-water solutions are made from Omnipur Glycerol (Calbiochem) at 65, 67 and 70 wt% (respectively Glyc-65, Glyc-67 and Glyc-70) to generate Newtonian fluids. In addition, the required amount of xanthan gum (Keltrol SF, CP Kelco) was stirred for 12 hours in

water to prepare 0.09, 0.11 and 0.14 wt% solutions (respectively XTN-0.09, XTN-0.11, XTN-0.14). These solutions are known to present a power-law behavior. The glycerol and xanthan gum solution properties (Table 2) were characterized by the protocol described in Section 2.5. The corresponding rheological curves are presented in Figure S1 and Figure S2.

Table 2: Newtonian and power-law fluid properties

	ρ (kg.m^{-3})	μ (mPa.s)		ρ (kg.m^{-3})	n	m (Pa.s^n)
Glyc-65	1179.3 ± 0.1	17.41 ± 0.06	**XTN-0.09**	1000	0.548	0.101
Glyc-67	1183.3 ± 0.4	20.05 ± 0.07	**XTN-0.11**	1000	0.532	0.129
Glyc-70	1192.0 ± 0.4	24.19 ± 0.08	**XTN-0.14**	1000	0.512	0.165

2.5. Experimental validation of dispersion state

The dispersion state may be easily evaluated by measuring the electrical conductivity of the suspension. Indeed, the ionic charges, which are present on the CNC surface due to the sulfate half ester groups, are released during sonication as the CNCs are individualized [30]. The conductivity value will increase accordingly until a maximum is reached. A baseline has been defined for batch conditions in our previous work [19] and is reported in the following section as targeted value for the semi-continuous setup. The conductivity is measured using an Oakton device (CON 6+) after observing a plateau of the pressure drop values to confirm that the well-dispersed state

for the given concentration has been obtained. These measurements are carried out in both beakers A and B to confirm the homogeneity of the dispersion.

All suspensions have been further analyzed using rheology to validate that the final dispersion state was the same as with a batch method. For this purpose, an Anton-Paar rheometer (MCR501) was used with a double Couette flow geometry. All tests were conducted at 25 °C unless specified otherwise. A pre-shear was applied for 100 s at 10 $s^{-1,}$ followed by a 180 s rest time. Then the dynamic viscosity was measured with a shear rate sweep from 500 s^{-1} to 0.5 s^{-1}.

The dispersion state was further validated by microscopy. Agglomerated spray-dried CNCs were observed with a Hitachi TM3030 Scanning Electron Microscope (SEM). The CNC-3.2 suspension dispersion state was then studied with a Talos™ L120 Transmission Electron Microscope (TEM) bright field imaging at 120kV just after complete CNC addition (36 $kJ.g^{-1}.L^{-1}$) and at the end of the process (60 $kJ.g^{-1}.L^{-1}$). To ensure proper observation, the suspensions were first diluted at 1 wt%, before being dried on a carbon coated-copper TEM grid (Electron Microscopy Sciences).

Finally, the densities of the glycerol solutions were measured using the Anton-Paar densimeter (DMA 4500M).

2.6. Numerical modeling

The fluid flow was modeled by the finite element COMSOL Multiphysics solver (version 5.5) to validate experiments and provide additional insight. The simulation considers a pipe diameter D, and a flow rate Q defined in Section 2.3. The static mixer has been modeled using the dimensions from Figure S3 and is placed at the same position as in the actual continuous setup, 5 cm after the first sensor. The distance between both sensors is L = 25 cm. Finally, the relative pressure at the entrance of the pipe is set to 381 Pa referring to the actual hydrostatic pressure. The fluid employed for the simulation part correspond to the Newtonian fluid Glyc-65 and the three power-law fluids (XTN-0.09, XTN-0.11, XTN-0.14) defined in Section 2.4). The Reynolds number for the power-law fluid Re_{PL} is defined as:

$$Re_{PL} = \frac{\rho v^{2-n} D^n}{m} \quad (1)$$

with v the fluid velocity and D is the pipe diameter. Reynolds number calculations (Table *3*) confirms a laminar regime (such as Re <10).

Table 3: Reynolds number

Fluid	Re
Glyc-65	6.9 ± 0.2
XTN-0.09	5.1 ± 0.2
XTN-0.11	4.2 ± 0.2
XTN-0.14	3.5 ± 0.2

Thus, using a laminar flow study in COMSOL, the Navier-Stokes equations are solved for an incompressible medium:

$$\rho(\boldsymbol{v}\cdot\nabla)\boldsymbol{v} = \nabla\left[-2pI + \mu\left((\nabla\boldsymbol{v}) + (\nabla\boldsymbol{v})^T\right)\right] \quad (2)$$

with p the fluid pressure and ρ and μ respectively the fluid density and Newtonian viscosity, assuming that the continuity equation is valid, defined by:

$$(\nabla\cdot\boldsymbol{v}) = 0 \quad (3)$$

In the case of non-Newtonian fluid following a power-law, μ is replaced by the dynamic viscosity η:

$$\eta = m\dot{\gamma}^{n-1} \quad (4)$$

in which $\dot{\gamma}$ is the shear rate.

2.7. Entry pressure estimation

The presence of a static mixer between the two sensors may imply an entry pressure ΔP_e that may be taken into using Bagley correction. To ease our calculations, we have kept the Newtonian model fluid (Glyc-65), with its corresponding viscosity and density. The flow rate is the same as for the CNC dispersion process, giving a laminar regime.

The wall stress τ_w may be determined by:

$$\tau_w = \mu \dot{\gamma}_e \quad (5)$$

with $\dot{\gamma}_e$ the effective shear rate. Then this wall stress is defined by:

$$\tau_w = D\left(\frac{\Delta P - \Delta P_e}{4L}\right) \quad (6)$$

where L is the pipe length and ΔP and ΔPe are respectively the pressure drop and the entry pressure.

2.8. Metzner and Otto concept

To calculate the in-line viscosity, it is possible to use the Metzner and Otto concept, which has been developed in the context of mechanical (impeller) stirring in the laminar regime, linking $\dot{\gamma}_e$ and the rotational speed N in the tank [26-28], using:

$$\dot{\gamma}_e = K_s N \quad (7)$$

where K_s is a geometry-dependent constant. This concept has been extended to static mixing, where the rotational speed is replaced by the characteristic fluid velocity in the pipe of characteristic dimension D:

$$\dot{\gamma}_e = K_s \frac{v}{D} \quad (8)$$

The constant K_s may then be calculated using the rheological properties of two power-law and Newtonian fluids, and the related pressure drops in the pipe $\Delta P_{(n)}$ and ΔP, respectively:

$$K_s = \frac{D}{v}\left[\frac{\Delta P_{(n)}}{\Delta P}\frac{\mu}{m}\right]^{\frac{1}{n-1}} \quad (9)$$

In this work, the constant K_s was determined for our system using the Newtonian and power-law fluids defined in Section 2.4, flowing in a laminar regime.

The power number, N_p, is known to be linked to the Reynolds numbers, Re and Re_{PL} (defined by equation (1)), for the Newtonian and power-law fluids, respectively, using the following relations:

$$K_p = N_p Re \quad (10)$$

$$K_{p(n)} = N_p Re_{PL} \quad (11)$$

where K_p and $K_{p(n)}$ are the so-called power constants, which depend on the static mixer geometry and power-law index n:

$$K_p = \frac{\Delta P D^2}{\mu L v} \quad (12)$$

$$K_{p(n)} = \frac{\Delta P_{(n)} D^{n+1}}{m L v^n} \quad (13)$$

Once they have been determined from experimental data, these constants can then be used to calculate K_s from equations (7), (11) and (12):

$$K_s = \left(\frac{K_{p(n)}}{K_p}\right)^{\frac{1}{n-1}} \quad (14)$$

This value for K_s can be compared with the one obtained for an empty tube (no static mixer) K_s' (calculations developed in Supplementary information 1), defined by:

$$K_s' = \frac{6n+2}{n} \quad (15)$$

Finally, the so-called process viscosity μ_{pr} for a power-law fluid, which is related to the Metzner and Otto concept, may be obtained from:

$$\mu_{pr} = m\left(\frac{K_s Q}{D^3}\right)^{n-1} \quad (16)$$

2.9. Surface modification with PEI

To expand the range of application for the experimental setup, surface modification on dispersed CNCs has been carried out. PEI was used for this purpose following the guidelines from Khandal et al. [29]. They observed indeed that ultrasonication was mandatory during PEI addition to prevent phase separation. A 1 wt% PEI solution was prepared by stirring the required amount of PEI in water at 50 ˚C for 30 min. After obtaining a 3.2 wt% CNC suspension with the previous protocol (CNC-3.2), this PEI solution was added dropwise in beaker B while ultrasonication was running to obtain (CNC/PEI-3.2). Sonication was maintained until a stable pressure drop value was obtained. To ensure that this additional ultrasonication treatment did not alter the CNCs, a reference experiment was conducted the same way without any PEI (CNC/noPEI-3.2). All preparation parameters are reported in Table 4.

Table 4: PEI addition parameters.

Name	CNC concentration (wt%)	PEI concentration (g/gCNC)	Additional ultrasonication treatment time (s)
CNC-3.2	3.2	-	-
CNC/noPEI-3.2	3.2	-	968
CNC/PEI-3.2	3.2	0.01	920

X-ray photoelectron spectroscopy (XPS) was employed on freeze-dried unmodified and modified CNCs to identify the presence of nitrogen. The instrument (XPS Axis UltraDLD, Kratos) was used with a monochromatic anode (225 W) and a charge neutralizer. The analyzed surface was 700*300 µm with a depth < 10 µm.

3. Results and discussion

3.1. Pressure drop measurements

The pressure drop has been calculated from the values obtained for each sensor as explained in Supplementary information 2. The raw data exhibited important oscillations resulting from several elements, namely the peristaltic pump. At the operating flow rate, the periodicity of the pump is ~2.23 s. As data values are acquired each 0.1 s, it was possible to filter some of the noise by determining a moving average on 22 points. Therefore, the standard deviation presented in this paper only considers

the setup sensitivity, neglecting pump variation. Other components of the setup, like the tubes which may be slightly flexible, as well as the sensor sensitivity indicated by the manufacturer, generate additional noise on the signal. It must also be noted that ultrasonication lead to bubble formation which, when transported into the tubes, induced measurable pressure fluctuations.

At t=0, the sensors only measure water and the values should be the same in all experiments. In our case, a slight variation has been observed which may be due to the sensitivity of the setup and the fact that water leads to a transitional-turbulent regime (Re = 102). Therefore, the pressure drop values have been normalized such as this initial value is around 0.

Figure 2 depicts the pressure drop measurements during the dispersion of the CNCs at 3 different concentrations. For each concentration, a plateau is observed after 13, 24 and 34 minutes respectively for 1.6, 3.2 and 4.8 wt% as reported in Table 5 (when the pressure drop oscillates around the same value ± 0.5 kPa for ~300 s). Additionally, whereas the pressure drop increases steadily for 1.6 and 3.2 wt% suspensions, an overshoot is seen with the highest concentration before reaching the plateau value. This may correspond to the dispersion homogenization time, more apparent at higher CNC loadings, with a higher local concentration.

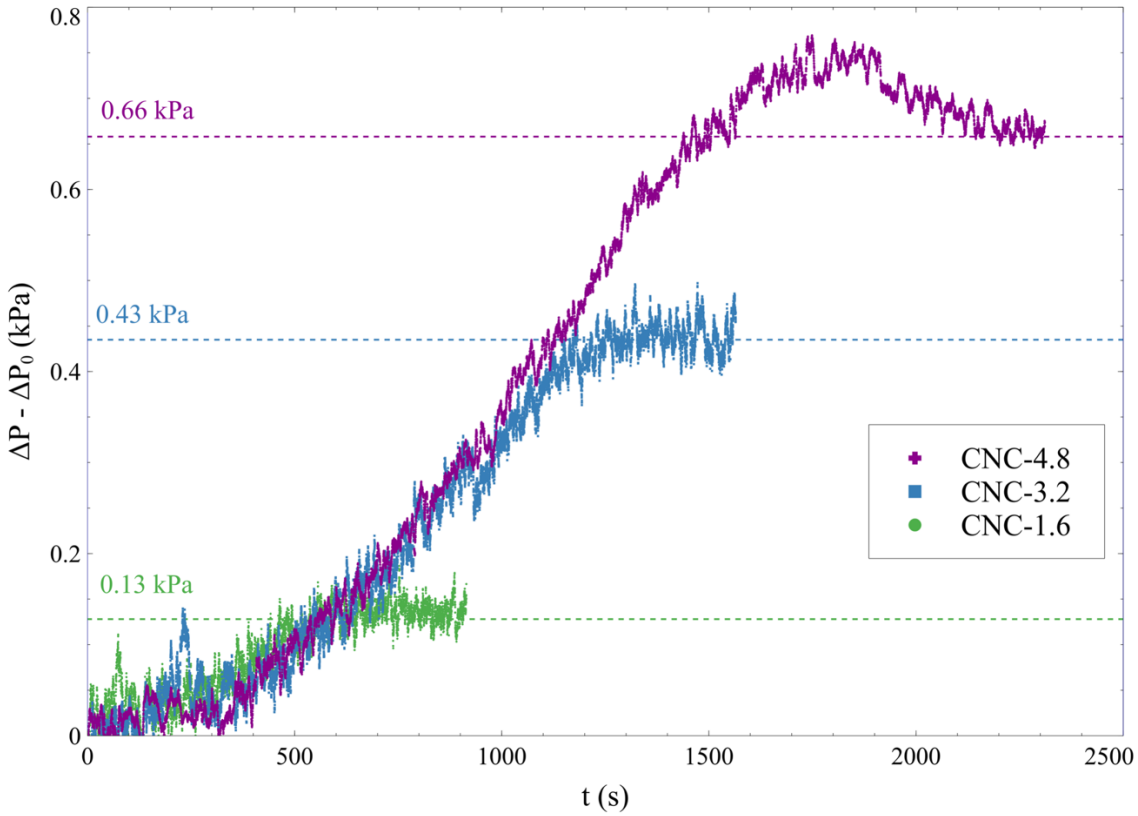

Figure 2: Pressure drop normalized by the initial value (water) of CNC suspensions as a function of process time. CNCs are added during the first minutes, and ultrasonication is initiated after 120 s.

Table 5 reports the overall energy applied to reach the final dispersion state. The ultrasonication energy is decreased by almost 2/3 compared to batch conditions (60 compared to 167 $kJ.g^{-1}.L^{-1}$). The energy brought by the pump is negligible in comparison, as it represents 10^{-5} times the ultrasonication energy. This gain in energy is mainly attributed to the gradual addition of CNCs in the beaker A, as the amount of CNCs to be dispersed at a given time becomes much lower than in batch. Moreover, the flow added by the peristaltic pump in beaker B provides additional beneficial

mixing. Although the change from continuous sonication (reference scenario) to pulsed mode (current case) was considered in the calculations, it may slightly impact the efficiency as well.

Table 5: Dispersion parameters.

Name	Total dispersion time (min)	Ultrasonication energy ($kJ.g^{-1}.L^{-1}$)	Pump energy ($J.g^{-1}.L^{-1}$)
CNC-1.6	13	60	0.9
CNC-3.2	24	60	0.9
CNC-4.8	34	60	0.9

3.2. Dispersion state validation with external tools

Reaching a pressure drop plateau must imply that the best dispersion conditions have been reached, and this should be sufficient to monitor the dispersion state. However, additional validation experiments could confirm that there is no loss of CNCs in the setup, or that its efficiency is not limited. For this purpose, conductivity and rheology have been used (Figure 3).

Figure 3a) plots the measured conductivity at the three studied concentrations obtained for the final dispersion state with the semi-continuous setup. The batch measurements are reported as a comparison. The targeted values have been reached for all concentrations, implying that the CNCs have indeed been well dispersed.

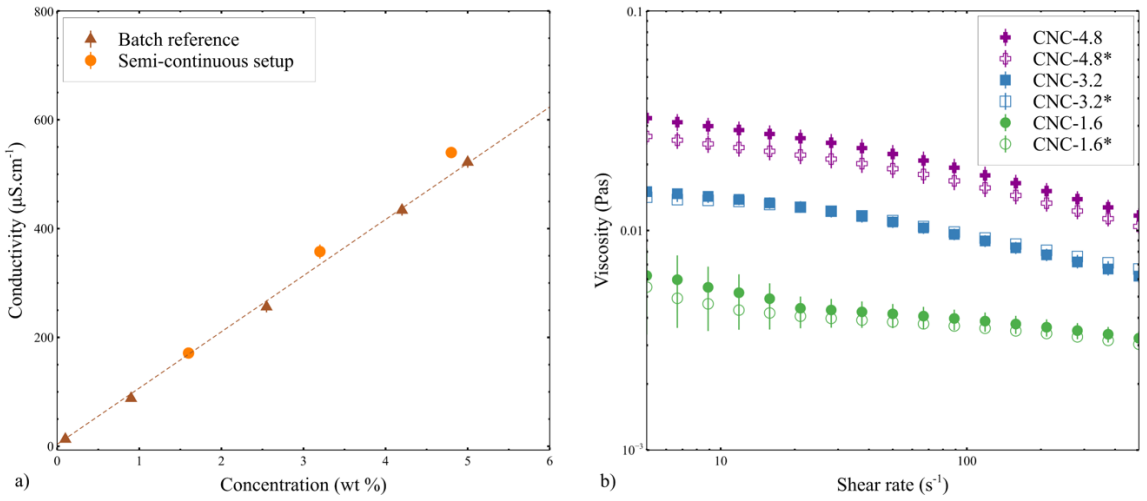

Figure 3: a) Conductivity as function of CNC concentration. Standard deviations are represented by vertical lines for the semi-continuous setup and is ± 10 µm for the batch reference. b) Viscosity of CNC ultrasonicated suspensions as function of shear rate (V = 60 mL, P = 65 W, E = 167 $kJ.g^{-1}.L^{-1}$) obtained either using a batch process (empty symbols) or the semi-continuous setup (full symbols). Standard deviations are represented by vertical lines.

Figure 3b) demonstrates that the viscosities as function of shear rate are the same for both dispersion methods. The highest concentration gives the largest difference between the batch and the semi-continuous path, while remaining within the standard deviation range. This may be explained because this concentration is close to the gel point (around 5 wt% [31]), where the viscosity is more time dependent. A slight delay between the preparation and the measurements may have impacted the results. Nevertheless, these measurements confirm that the desired dispersion state has been obtained.

Eventually, this statement was validated by microscopy (Figure S5). When observing the spray-dried CNCs by SEM, larger agglomerates on the order of 100 μm are clearly visible. For CNC-3.2, upon dispersion under poor conditions (after 18 min and E = 36 kJ.g^{-1}.L^{-1}) in the semi-continuous setup, partial dispersion is detected, though CNC bundles remain apparent by TEM. Then at the final state (E = 36 kJ.g^{-1}.L^{-1}), CNCs are now more individualized.

3.3. Dispersion state validation using in-line measurements

While pressure drop measurements may give enough information to conclude on adequate dispersion state, additional analysis can provide more direct insight into the viscosity of the system, without the need for external validation.

3.3.1. Effective shear rate and entry pressure

The numerical modeling of the tube between the pressure sensors described in Section 2.6 provides an estimation of several flow parameters for a 65 wt% glycerol solution (Glyc-65). Accordingly, the effective shear rate obtained by modeling $\dot{\gamma}_e$ is 52.5 s^{-1}. In addition, it comes from the pressure profile (Figure S6) that the pressure drop ΔP_m between the two sensors is 0.915 kPa. We must note that this value is determined by point estimation (rather than surface average) as the sensors measure the pressure locally in our setup. The experimental value ΔP_{exp} for the same fluid is 1.4 ± 0.1 kPa, which is higher than the prediction. It may be due to additional effects not considered in the simulation, such as the pulsing of the peristaltic pump.

In both cases, it is then possible to quantify the entry pressure using equations (5) and (6) (Table 6). For the purposes of these calculations, the $\dot{\gamma}_e$ value retained is extracted from the simulation – this value will be validated experimentally in Section 3.3.2. A higher total pressure drop value is measured experimentally (ΔP_{exp}) leading logically to a higher entry pressure, compared to the modeling value (ΔP_m).

Table 6 : Entry pressure estimation for Glyc-65.

	Modeling	Experiment
μ (mPa.s)	17.41 ± 0.06	-
$\dot{\gamma}_e$ (s^{-1})	52.5	-
τ_w (Pa)	0.914	-
ΔP_m or ΔP_{exp} (kPa)	0.915	1.4 ± 0.1
ΔP_e (kPa)	0.723	1.2 ± 0.1

Nevertheless, modeling and experiments lead to the same conclusion: the entry pressure is considerable ($\Delta P_e/\Delta P_{exp}$ = 86%). One solution that will diminish the impact of this entry pressure is to increase the distance between the two sensors. However, by doubling the distance, the result remains unacceptable (for L = 59.4 cm, $\Delta P_e/\Delta P_{exp}$ = 76%), and a longer tube will cause practical problems (i.e. increased volume in tubing). In addition, this effect is fluid dependent, so it is challenging to predict. For

all these reasons, the pressure drop measured by the sensors cannot directly provide a viscosity value simply using capillary flow analysis.

3.3.2. Process viscosity

However, using equation (16) defined in Section 2.8, it is possible to determine the process viscosity depending only on the setup geometry. To do so, the Newtonian and power-law fluids stated in Section 2.4 are introduced in the semi-continuous setup, and the pressure drop is measured at different flow rates (Figure S7).

Using equations (12) and (13), the constants K_p and $K_{p(n)}$ were calculated (Table 7). As expected, $K_{p(n)}$ depends on n whereas K_p is constant for all the Newtonian fluids considered. K_s was then deduced from these results using equation (14), with an average value of all glycerol solutions for K_p. For this system, $K_s = 12$. K_s' is also calculated for a comparison purpose: $K_s > K_s'$ as the static mixer implies additional shear in the pipe.

Table 7: Metzner and Otto analogy calculations using Newtonian and power-law fluids.

	n	K_p or $K_{p(n)}(10^1)$	K_s	K_s'
Glyc-65	1	33 ± 7	-	
Glyc-67	1	34 ± 6	-	8.0
Glyc-70	1	30 ± 4	-	
XTN-0.09	0.548	11 ± 3	11 ± 10	9.7

XTN-0.11	0.532	10 ± 3	12 ± 10	9.8
XTN-0.14	0.512	9 ± 2	13 ± 10	9.9

It is important to note that for the 65 wt% glycerol solution, this value of K_s gives an average effective shear rate of $\dot{\gamma_e} = 53 \pm 50\ s^{-1}$ with equation (8) and $Q = 3.8*10^{-7}\ m^3.s^{-1}$. Therefore, even if the standard deviation is high due to the sensor sensitivity, the simulation gives a similar result (52.5 s^{-1}), confirming the reliability of the method. Moreover, the effective shear rate for the corresponding empty tube is 44 s^{-1}. This agrees with the fact that adding a static mixer in the pipe leads to additional obstruction and more shear.

An additional validation has been performed using the numerical modeling presented in Section 2.6 on each power law fluids and Glyc-65. The pressure drop was estimated and K_s was obtained with Equation (9). For this system, $K_s = 18$ which confirms again the consistency of our results, being in the same order of magnitude as the experimental value.

Once our system parameters were clearly defined, the same method was applied for the CNC suspensions. The 3.2 wt% concentration is here chosen as an example. As a reference, the same concentration obtained in batch (CNC-3.2*) was characterized at 35 °C using rheology. The CNC suspension does not display a power-flow behaviour over the entire shear rate range. Thus, while the shear rate in the tube is not constant,

the average value determined above (53 s^{-1}) is used to obtain the parameters *n* and *m* and the targeted viscosity reported in Table 8 (see Figure S8 for the rheological data).

Table 8 : Rheological properties of the 3.2 wt% CNC suspension obtained in batch

	n	m	η (mPa.s) at 53 s^{-1}
CNC-3.2*	0.767	0.0212	8.4 ± 0.1

Then, $K_{p(n)}$ was calculated using the pressure drop that was obtained at the end of the dispersion using the semi-continuous setup for CNC-3.2 (ΔP-ΔP_0 = 0.43 kPa). Next, K_s was estimated, leading to the process viscosity (Equation (16)). All results are presented in Table 9. We may note that the standard deviation is quite large, considering the pressure sensor sensitivity. However, the modeling comparison in this section has demonstrated the reliability of the method.

Table 9: Process viscosity calculation for the 3.2 wt% CNC suspension

Dispersion time	ΔPn (kPa)	$K_{p(n)}$ (10^1)	K_s	μ_{pr} (mPa.s)
24 min	0.7 ± 0.1	18 ± 5	11 ± 20	9 ± 70

At the same shear rate, the dynamic viscosity of CNC-3.2* obtained using rheology is close to the value determined experimentally, which confirms that the final dispersion state at 24 minutes is the desired one. Note that in case of a bad dispersion, it would have given a different value of K_s even if *m* and *n* from CNC-3.2*, considered as an optimal dispersion, are used It must be emphasized that this could be obtained

without external validation. Such a process viscometry method can thus be transposed to a variety of fluids or concentrations with the same setup, provided initial in-line measurements on known fluids are conducted, as it is mainly dependent on geometry.

3.4. Surface modification

3.4.1. PEI addition

PEI addition was monitored via pressure measurements. Figure 4 illustrates the pressure drop values as function of dispersion time. Below 1570 s is the initial dispersion stage and the red line in the figure separates it from the PEI addition step. As expected, the addition of PEI leads to a fast increase of the pressure drop (see CNC/PEI-3.2) due to the viscosity increase. The CNC dispersion undergoing the same sonication without PEI addition (CNC/noPEI-3.2) shows a pressure drop oscillating around the plateau value (0.43 kPa) reached after the final dispersion state. This confirms that no further change is made on the CNC dispersion with the additional ultrasonication time.

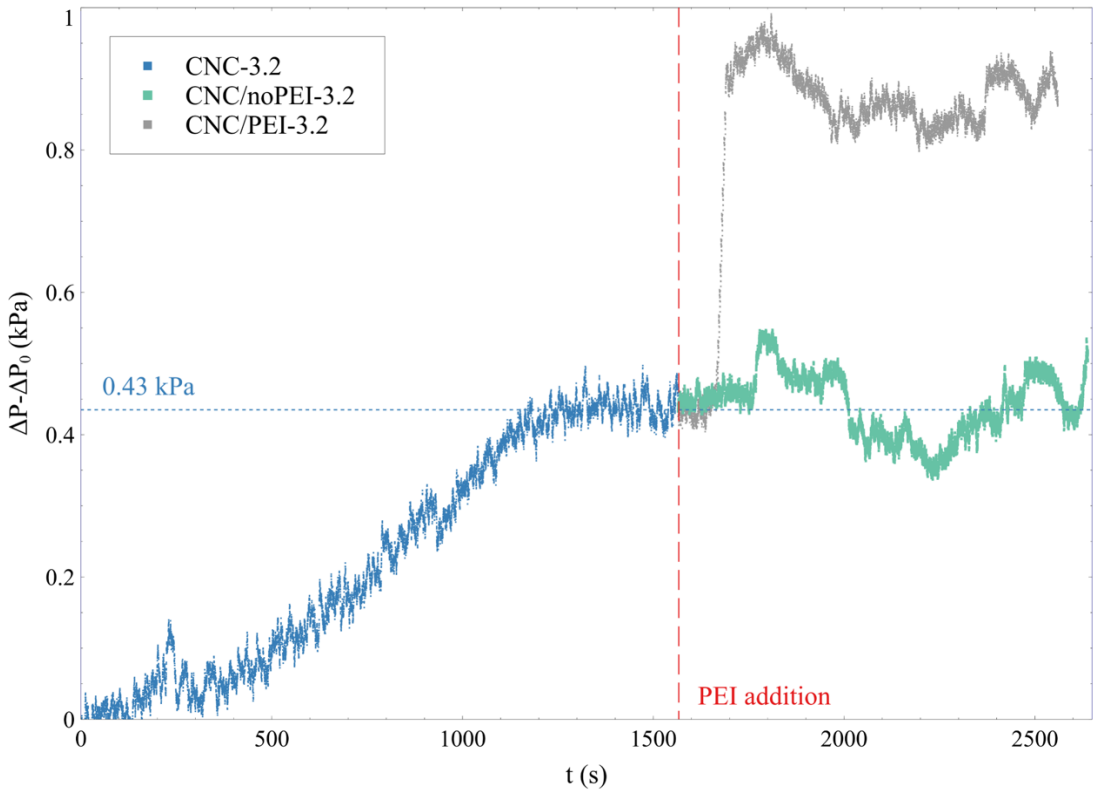

Figure 4: Pressure drop of CNC suspensions as function of process time. CNCs are added during the 60 s, and ultrasonication is started after 120 s. At t=1570 s, the CNC dispersions are further ultrasonicated with or without PEI addition.

The ultrasonication energy applied to complete the PEI addition was based on the work of Khandal et al. [29] who was working in a batch mode. Because the semi-continuous setup provides a gain of efficiency, only 36% of the suggested energy amount has been applied. Yet, no drastic change is observed on ΔP after the first five minutes following the addition. The purpose of this experiment was to prove that our setup could be used for CNC modification. However, an optimization study on the ultrasonication energy needed in this step may be relevant.

Figure 5 depicts the viscosity of the different suspensions as function of shear rate. The results confirmed what was observed in Figure 4: the CNC suspension with additional ultrasonic energy but no PEI (CNC/noPEI-3.2) presents the same viscosity as the initial CNC suspension (CNC-3.2). A slight increase in viscosity is noted for the modified CNC suspension (CNC/PEI-3.2 (fresh)) when analyzed just after the dispersion. After 13 days, this suspension demonstrates a shear thinning behavior, typical of a gel-like suspension. This rheopexy concurs with Khandal et al.'s observations [29], validating the success of the PEI physical adsorption on CNCs. Additionally, XPS analyses has been carried out to confirms nitrogen presence at 0.3%, close to the theorical value of 0.32% (Figure S9).

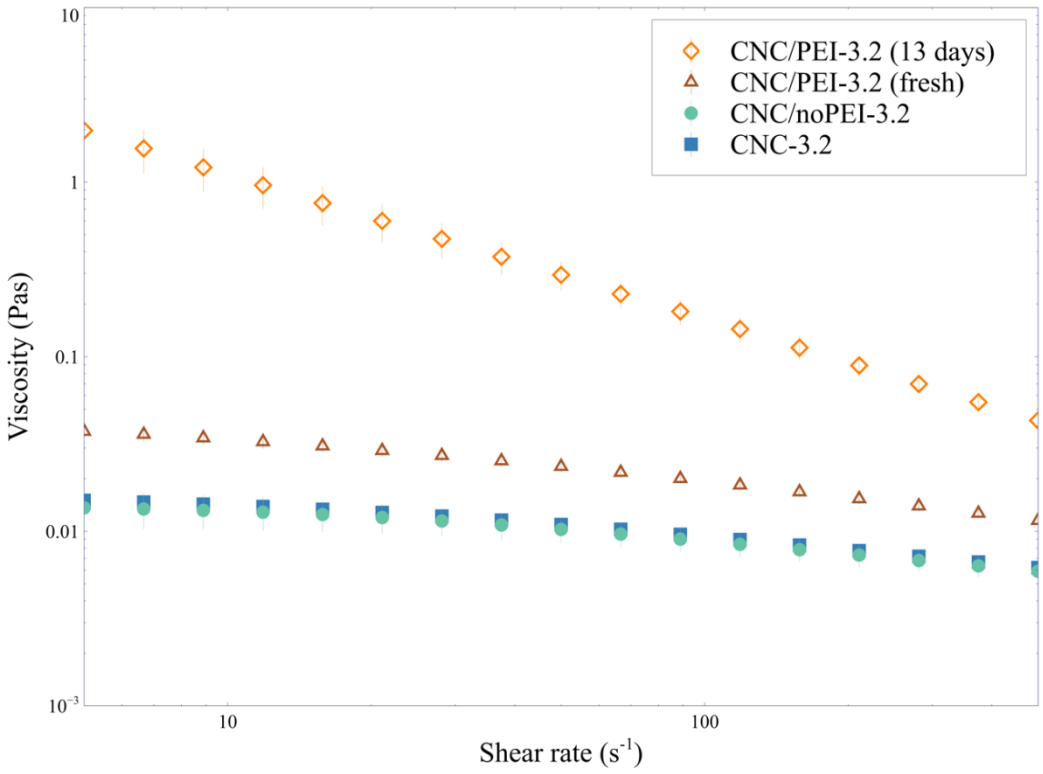

Figure 5: Viscosity of CNC ultrasonicated suspensions as function of shear rate (V = 60 mL, P = 15 (65) W, E = 167 kJ.g^{-1}.L^{-1}) after dispersion or with further ultrasonication with/without PEI addition.

4. Conclusion

The semi-continuous setup used in this work offers a successful method to adapt the optimized batch ultrasonication procedure to larger volumes using standard probe. By maintaining the volume directly exposed to ultrasonication the same as what was suggested in a smaller batch (60 mL), continuously fed by a larger to-be-dispersed volume, it was possible to achieve a well-dispersed state with an excellent gain in energy efficiency (64% less energy than required in batch). This approach provides the additional asset of working with an ultrasonication probe without additional significant

infrastructure costs. Pressure sensors provided direct information on the dispersion state with a simple in-line measurement read-out: a stable value implying the final state has been reached. However, through a more in-depth analysis, it is also possible to extract the process viscosity, confirming that the desired CNC dispersion has been reached without additional analyses validation or sampling. Thus, this ensures for example that no CNCs have remained stuck on the tank wall. This method may then be applied to different systems as long as the setup parameters are known. The dispersion state may also be quantified by conductivity, but contrary to the pressure measurements and viscosity estimation, this technique can only be used in case of charged particles (such as CNCs). We have further shown that this setup can be used for surface modification, using the example of PEI adsorption.

This work may be adapted at other scales, especially since the constant K_s used for process viscosity calculation remains the same. Indeed, once the so-called Metzner and Otto constant K_s is known, it is possible to estimate the parameters n and m of any power-law fluid using an additional static mixer. It was however not the scope of the present work. Nevertheless, it would be interesting to study the shear rate values for different system dimensions and evaluate the limits of the comparison made between the viscosity obtained in rheology and the process viscosity. In addition to surface modification, the semi-continuous setup could also be exploited for other applications after validating the dispersion state, such as Pickering emulsion preparation. Finally, as

the method does not depend on CNC properties, it is realistic to suggest that it may be used for other nanoparticle dispersion.

Acknowledgments: The authors are grateful for the National Science and Engineering Research Council of Canada (NSERC), namely its CRD and CREATE programs, Prima Québec and FPInnovations for their financial support. The authors also acknowledge Celluforce for providing the cellulose nanocrystals. Additionally, we would like to thank CREPEC for the expertise and infrastructure access, and the Simulation-based Engineering Science (Génie Par la Simulation) group for scholarship support. Moreover, we would like to thank S. Chenard and M. Beaudoin for their help on the flow setup and the data acquisition system.

[1] X. Feng, Z. Yang, S. Chmely, Q. Wang, S. Wang, and Y. Xie, "Lignin-coated cellulose nanocrystal filled methacrylate composites prepared via 3D stereolithography printing: Mechanical reinforcement and thermal stabilization," *Carbohydr Polym,* vol. 169, pp. 272-281, Aug 1 2017, doi: 10.1016/j.carbpol.2017.04.001.

[2] Z. Zhang, M. Cheng, M. S. Gabriel, A. A. Teixeira Neto, J. da Silva Bernardes, R. Berry, and K. C. Tam, "Polymeric hollow microcapsules (PHM) via cellulose nanocrystal stabilized Pickering emulsion polymerization," *J Colloid Interface Sci,* vol. 555, pp. 489-497, Nov 1 2019, doi: 10.1016/j.jcis.2019.07.107.

[3] R. Moon, S. Beck, and A. Rudie, "Cellulose Nanocrystals – A Material with Unique Properties and Many Potential Applications," in *Production and Applications of Cellulose Nanomaterials*: TAPPI Press, 2013, ch. 1.

[4] N. B. Palaganas, J. D. Mangadlao, A. C. C. de Leon, J. O. Palaganas, K. D. Pangilinan, Y. J. Lee, and R. C. Advincula, "3D Printing of Photocurable Cellulose Nanocrystal Composite for Fabrication of Complex Architectures via Stereolithography," *ACS Appl Mater Interfaces,* vol. 9, no. 39, pp. 34314-34324, Oct 4 2017, doi: 10.1021/acsami.7b09223.

[5] R. J. Moon, A. Martini, J. Nairn, J. Simonsen, and J. Youngblood, "Cellulose nanomaterials review: structure, properties and nanocomposites," *Chem Soc Rev,* vol. 40, no. 7, pp. 3941-94, Jul 2011, doi: 10.1039/c0cs00108b.

[6] J. Huang, A. Dufresne, and N. Lin, Eds. *Nanocellulose: From Fundamentals to Advanced Materials, First Edition*. John Wiley & Sons Inc., 2019.

[7] W. Y. Hamad and T. Q. Hu, "Structure-process-yield interrelations in nanocrystalline cellulose extraction," *The Canadian Journal of Chemical Engineering,* pp. n/a-n/a, 2010, doi: 10.1002/cjce.20298.

[8] J. Araki, M. Wada, S. Kuga, and T. Okano, "Flow properties of microcrystalline cellulose suspension prepared by acid treatment of native cellulose," *Colloids and Surfaces A: Physicochemical and Engineering Aspects,* vol. 142, no. 1, pp. 75-82, 1998, doi: 10.1016/s0927-7757(98)00404-x.

[9] N. Wang, E. Y. Ding, and R. S. Cheng, "Thermal degradation behaviors of spherical cellulose nanocrystals with sulfate groups," (in English), *Polymer,* vol. 48, no. 12, pp. 3486-3493, Jun 4 2007, doi: 10.1016/j.polymer.2007.03.062.

[10] E. J. Foster, R. J. Moon, U. P. Agarwal, M. J. Bortner, J. Bras, S. Camarero-Espinosa, K. J. Chan, M. J. D. Clift, E. D. Cranston, S. J. Eichhorn, D. M. Fox, W. Y. Hamad, L. Heux, B. Jean, M. Korey, W. Nieh, K. J. Ong, M. S. Reid, S. Renneckar, R. Roberts, J. A. Shatkin, J. Simonsen, K. Stinson-Bagby, N. Wanasekara, and J. Youngblood, "Current characterization methods for cellulose nanomaterials," *Chem Soc Rev,* vol. 47, no. 8, pp. 2609-2679, Apr 23 2018, doi: 10.1039/c6cs00895j.

[11] X. M. Dong and D. G. Gray, "Effect of Counterions on Ordered Phase Formation in Suspensions of Charged Rodlike Cellulose Crystallites," *Langmuir,* vol. 13, no. 8, pp. 2404-2409, 1997, doi: 10.1021/la960724h.

[12] Y. C. Peng, D. J. Gardner, Y. Han, A. Kiziltas, Z. Y. Cai, and M. A. Tshabalala, "Influence of drying method on the material properties of nanocellulose I:

thermostability and crystallinity," (in English), *Cellulose,* vol. 20, no. 5, pp. 2379-2392, Oct 2013, doi: 10.1007/s10570-013-0019-z.

[13] Q. Beuguel, J. R. Tavares, P. J. Carreau, and M. C. Heuzey, "Ultrasonication of spray- and freeze-dried cellulose nanocrystals in water," *J Colloid Interface Sci,* vol. 516, pp. 23-33, Apr 15 2018, doi: 10.1016/j.jcis.2018.01.035.

[14] V. Khoshkava and M. R. Kamal, "Effect of drying conditions on cellulose nanocrystal (CNC) agglomerate porosity and dispersibility in polymer nanocomposites," (in English), *Powder Technology,* vol. 261, pp. 288-298, Jul 2014, doi: 10.1016/j.powtec.2014.04.016.

[15] Y. Y. Huang and E. M. Terentjev, "Dispersion of Carbon Nanotubes: Mixing, Sonication, Stabilization, and Composite Properties," (in English), *Polymers,* vol. 4, no. 1, pp. 275-295, Mar 2012, doi: 10.3390/polym4010275.

[16] J. S. Taurozzi, V. A. Hackley, and M. R. Wiesner, "Ultrasonic dispersion of nanoparticles for environmental, health and safety assessment--issues and recommendations," *Nanotoxicology,* vol. 5, no. 4, pp. 711-29, Dec 2011, doi: 10.3109/17435390.2010.528846.

[17] K. S. Suslick, "Sonochemistry," in *Kirk-Othmer Encyclopedia of Chemical Technology*, vol. 26, I. John Wiley & Sons Ed., Fourth ed. New-York, 1998, pp. 516-541.

[18] S. K. Bhangu and M. Ashokkumar, "Theory of Sonochemistry," *Top Curr Chem (Cham),* vol. 374, no. 4, p. 56, Aug 2016, doi: 10.1007/s41061-016-0054-y.

[19] M. Girard, D. Vidal, F. Bertrand, J. R. Tavares, and M. C. Heuzey, "Evidence-based guidelines for the ultrasonic dispersion of cellulose nanocrystals," *Ultrason Sonochem,* vol. 71, p. 105378, Mar 2021, doi: 10.1016/j.ultsonch.2020.105378.

[20] M. Girard, F. Bertrand, J. R. Tavares, and M. C. Heuzey, "Rheological insights on the evolution of sonicated cellulose nanocrystal dispersions," *Ultrason Sonochem,* vol. 78, p. 105747, Oct 2021, doi: 10.1016/j.ultsonch.2021.105747.

[21] R. F. Contamine, A. M. Wilhelm, J. Berlan, and H. Delmas, "Power Measurement in Sonochemistry," (in English), *Ultrasonics Sonochemistry,* vol. 2, no. 1, pp. S43-S47, May 1995, doi: Doi 10.1016/1350-4177(94)00010-P.

[22] A. Peshkovsky, "From Research to Production: Overcoming Scale-Up Limitations of Ultrasonic Processing," in *Ultrasound: Advances for Food Processing and Preservation*, 2017, ch. 17, pp. 409-423.

[23] S. L. Peshkovsky and A. S. Peshkovsky, "High capacity ultrasonic reactor system," United States Patent US8651230B2, 2008.

[24] U. C. Lohani and K. Muthukumarappan, "Study of continuous flow ultrasonication to improve total phenolic content and antioxidant activity in sorghum flour and its comparison with batch ultrasonication," *Ultrasonics Sonochemistry,* vol. 71, 2021, doi: 10.1016/j.ultsonch.2020.105402.

[25] J. Carpenter, S. George, and V. K. Saharan, "A comparative study of batch and recirculating flow ultrasonication system for preparation of multilayer olive oil in water emulsion stabilized with whey protein isolate and sodium alginate," *Chemical Engineering and Processing - Process Intensification,* vol. 125, pp. 139-149, 2018, doi: 10.1016/j.cep.2018.01.006.

[26] A. Arzate, F. Bertrand, O. Reglat, and P. Tanguy, "Apparatus and method for measuring the rheological properties of a power law fluid," Patent Appl. 09/493,414, 2002.
[27] A. Arzate, "Détermination de la viscosité en ligne des sauces de couchage de papier," Master, Chemical Engineering, Polytechnique Montreal, Quebec, Canada, 1999.
[28] A. B. Metzner and R. E. Otto, "Agitation of non-Newtonian fluids," *AIChE Journal,* vol. 3, no. 1, pp. 3-10, 1957, doi: 10.1002/aic.690030103.
[29] D. Khandal, B. Riedl, J. R. Tavares, P. J. Carreau, and M.-C. Heuzey, "Tailoring cellulose nanocrystals rheological behavior in aqueous suspensions through surface functionalization with polyethyleneimine," *Physics of Fluids,* vol. 31, no. 2, 2019, doi: 10.1063/1.5046669.
[30] S. Beck, J. Bouchard, and R. Berry, "Controlling the reflection wavelength of iridescent solid films of nanocrystalline cellulose," *Biomacromolecules,* vol. 12, no. 1, pp. 167-72, Jan 10 2011, doi: 10.1021/bm1010905.
[31] Y. Xu, A. D. Atrens, and J. R. Stokes, "“Liquid, gel and soft glass” phase transitions and rheology of nanocrystalline cellulose suspensions as a function of concentration and salinity," *Soft Matter,* vol. 14, no. 10, pp. 1953-1963, 2018, doi: 10.1039/c7sm02470c.

Supplementary data

Supplementary information 1: Determination of K_s for an empty tube

For a power-law fluid in a pipe, Poiseuille law is defined such as:

$$Q = \frac{\pi R^3}{\frac{1}{n}+3}\left[\frac{R\Delta P}{2nL}\right]^{\frac{1}{n}} \quad \text{(S1)}$$

According to this equation, $K_{p(n)}$ may be calculated from equation (11) giving:

$$K_{p(n)} = A^n \frac{2^{n+2}R^n}{V^n} \quad \text{(S2)}$$

with A defined by:

$$A = \frac{\left(\frac{1}{n}+3\right)Q}{\pi R^3} \quad \text{(S3)}$$

Then, using the same notation, K_p may be estimated from equation (12) such as:

$$K_{p(n)} = \frac{2^3 AR}{v} \quad \text{(S4)}$$

Ks formula is thus obtained from equations (14), (S2) and (S4) :

$$K_s = 6 + \frac{2}{n} \quad \text{(S5)}$$

Supplementary information 2: Pressure sensors calibration

The pressure sensors provide an output signal proportional to the measured pressure. The pressure value P (in kPa) and the output signal V_{out} (in V) are correlated by the manufacturer with the following formula:

$$V_{out} = V_s(0.2P + 0.5) \quad \text{(S6)}$$

where $V_s = 5.0 \pm 0.25$ V is the supply voltage This equation has been validated with hydrostatic pressure measurements using a water column. For both sensors, there is a slight deviation between the two methods (Figure S4), so the equation (S6) was modified as follows:

$$V_{out} = 0.84P + 2.67 \quad \text{(S7)}$$

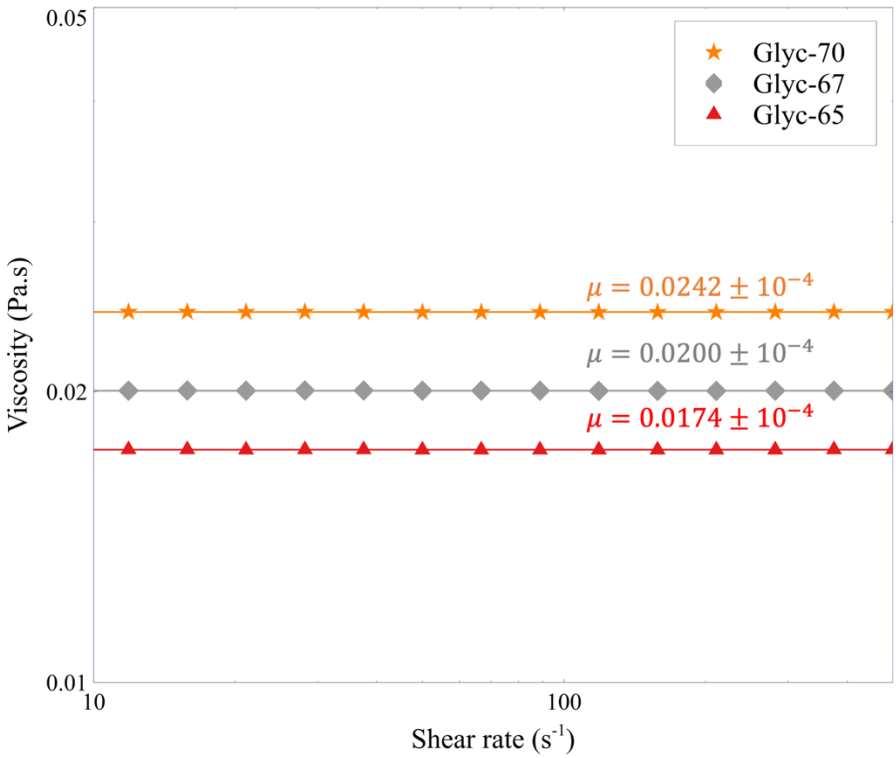

Figure S1: Viscosity of glycerol water-based solutions at 65, 67 and 70 wt% as function of shear rate

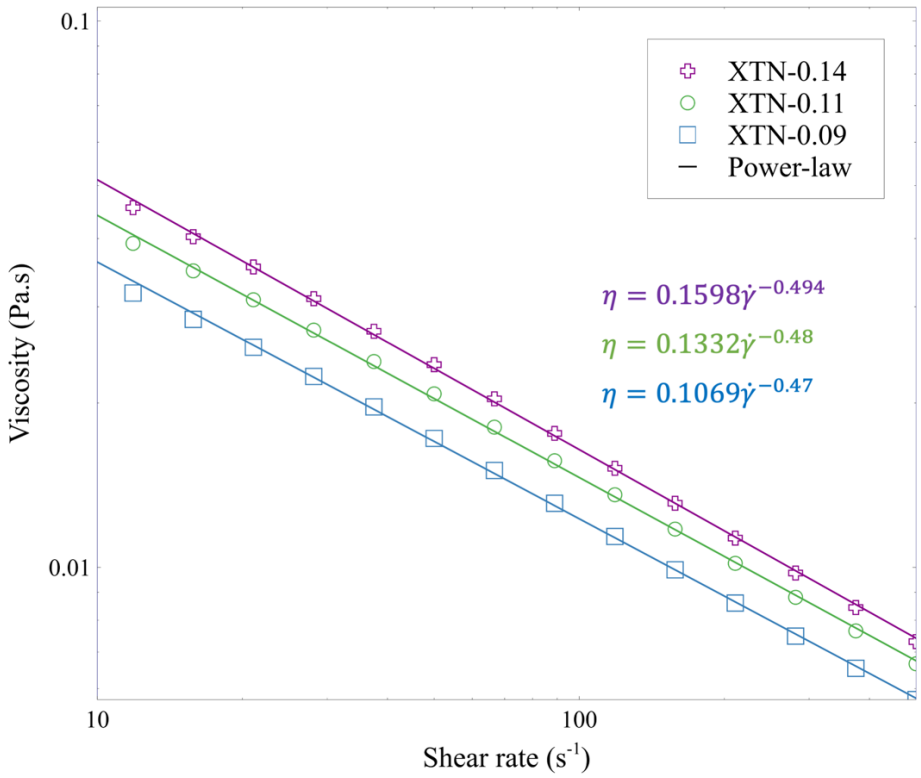

Figure S2: Viscosity of xanthan water-based solutions at 0.09, 0.11 and 0.14 wt% as function of shear rate with a power-law fitting

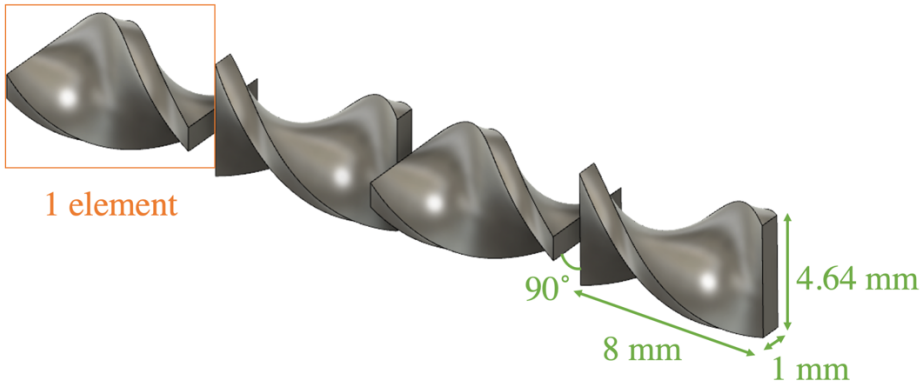

Figure S3: Static mixer dimensions. Four elements out of 23 are represented for clarity purpose.

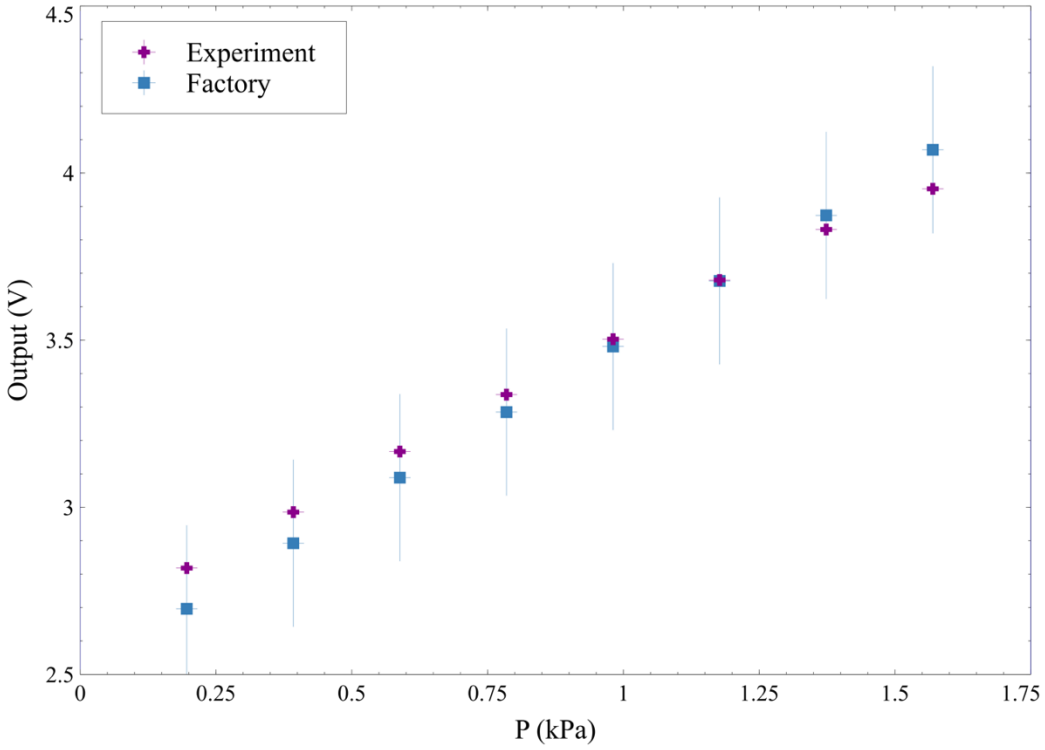

Figure S4: Calibration of the pressure sensors. Both sensors were experimentally giving the same behavior, and the obtained values are compared with the factory calibration

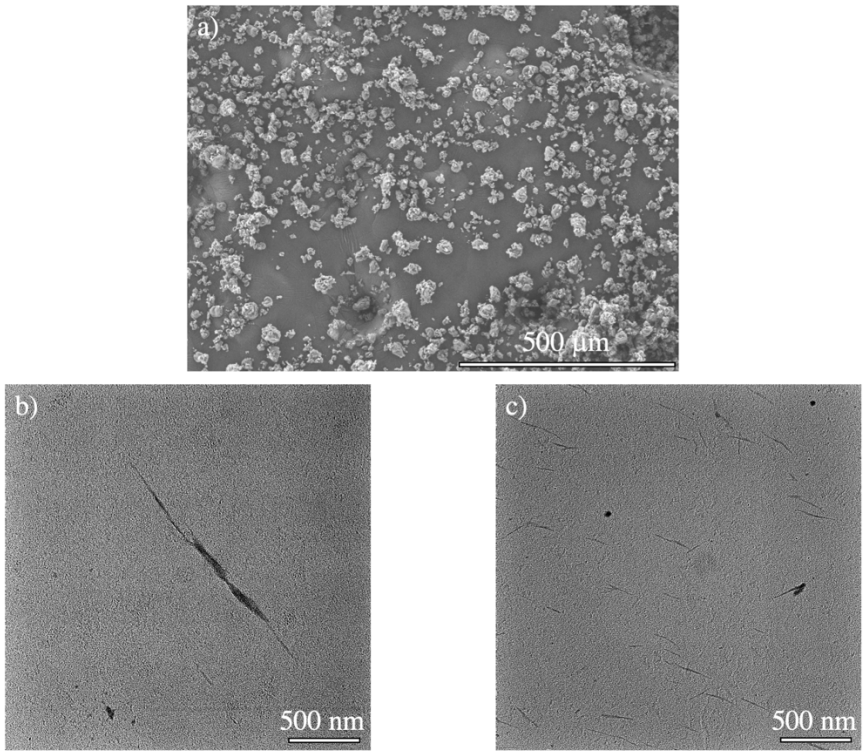

Figure S5: a) Spray-dried CNCs SEM image and TEM images of a CNC-3.2 processed with the semi-continuous setup with: b) CNC bundle at E = 36 $kJ.g^{-1}.L^{-1}$ and c) individualized CNC at E = 60 $kJ.g^{-1}.L^{-1}$

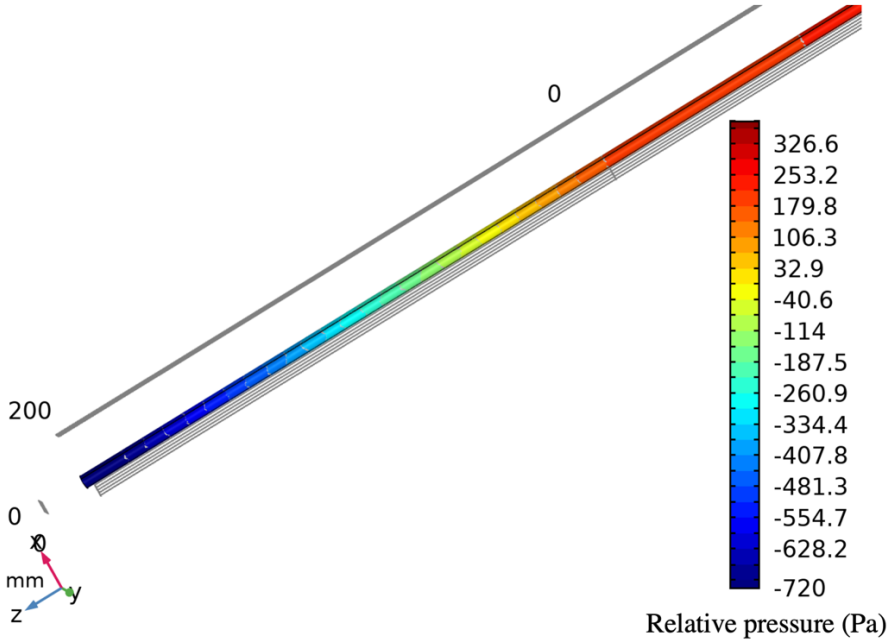

Figure S6: Relative pressure field related to the 65 wt% glycerol solution flow in the semi-continuous setup modeling: (flow direction in positive z-direction, pressure sensors placed at z = - 50 mm and z = 200 mm, static mixer placed at z = 0 mm)

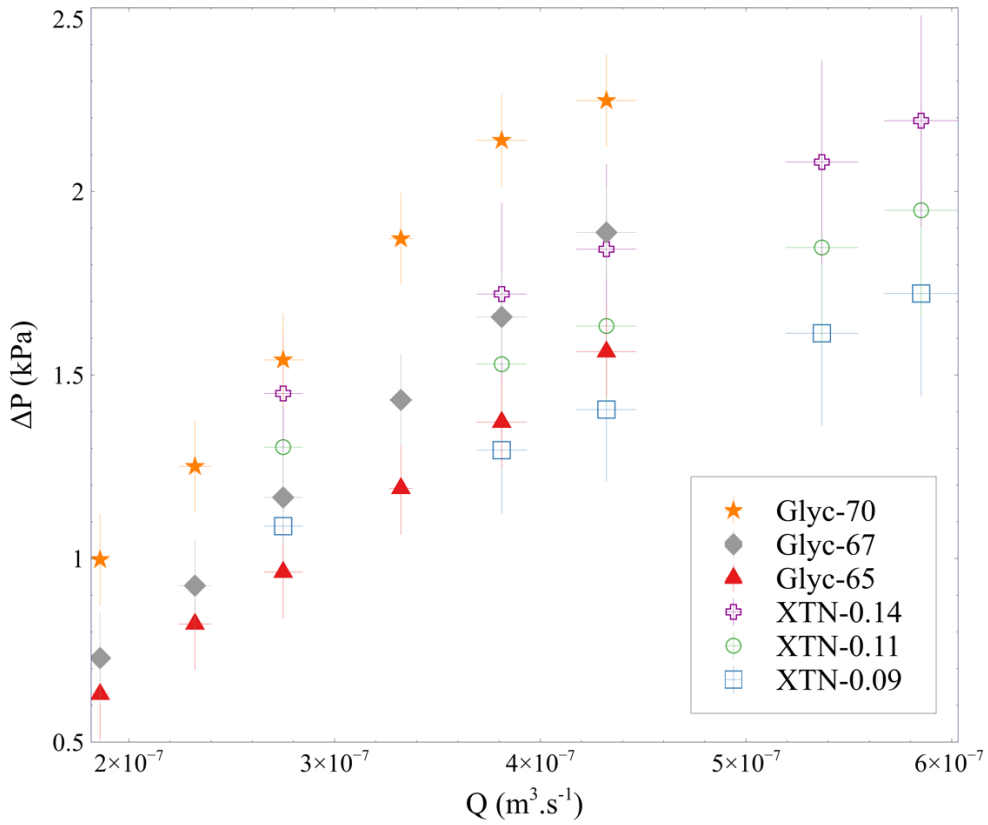

Figure S7: Pressure drop as function of flow rate measured in the semi-continuous setup

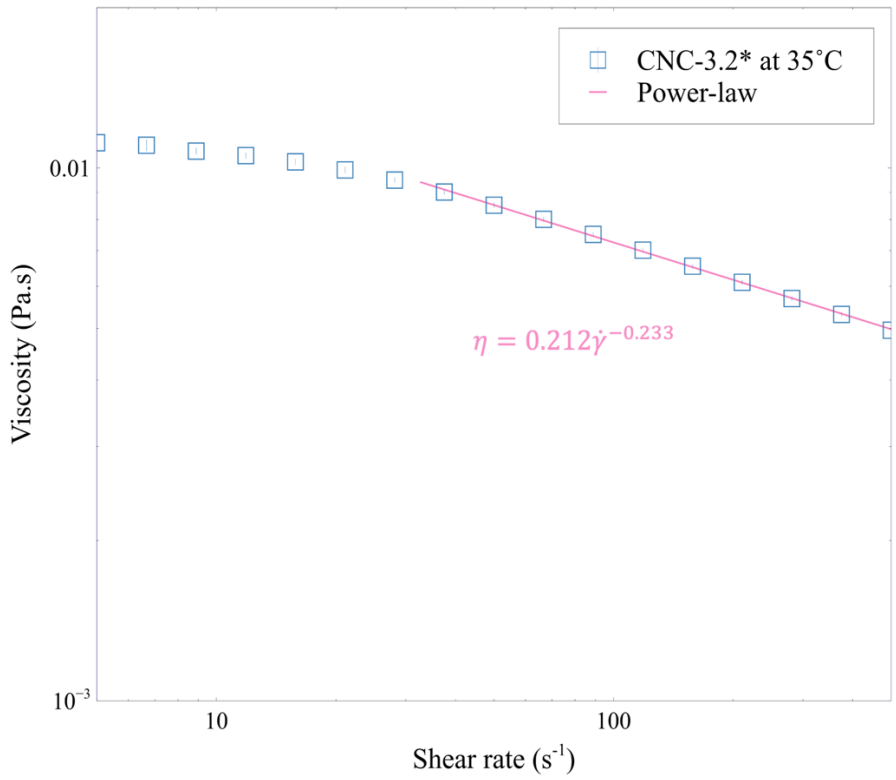

Figure S8: Viscosity of a 3.2 wt% CNC ultrasonicated batch suspension (V = 60 mL, P = 15 (65) W, E = 167 $kJ.g^{-1}.L^{-1}$) as function of shear rate at 35 °C with a power-law fitting at high shear rate

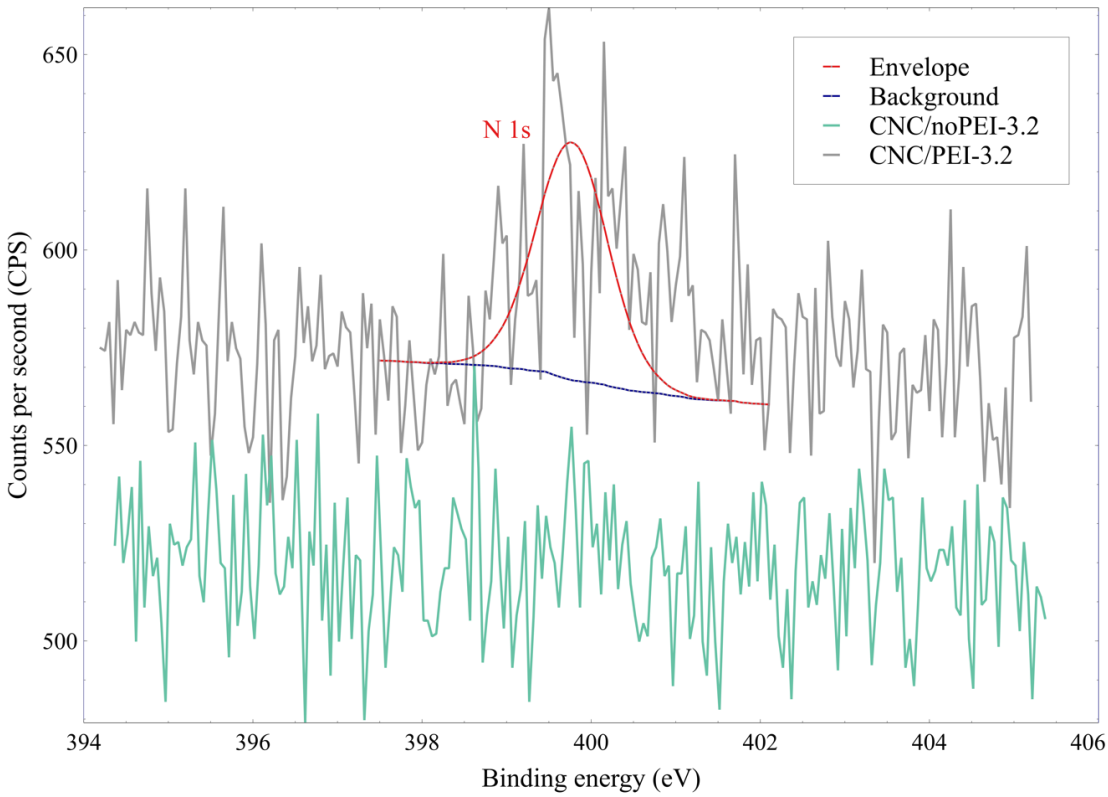

Figure S9: XPS graph of freeze-dried CNC/noPEI-3.2 and CNC/PEI-3.2. The high signal-to-noise ratio is attributed to the low content of nitrogen for the modified CNC (~ 0.3%)